Metagenomic analysis of ecological niche overlap and community collapse in microbiome dynamics

Hiroaki Fujita[1†], Masayuki Ushio[1,2], Kenta Suzuki[3], Masato S. Abe[4], Masato Yamamichi[5,6], Yusuke Okazaki[7], Alberto Canarini[1], Ibuki Hayashi[1], Keitaro Fukushima[8], Shinji Fukuda[9-12], E. Toby Kiers[13], and Hirokazu Toju[1†]

[1]Center for Ecological Research, Kyoto University, Otsu, Shiga 520-2133, Japan

[2]Department of Ocean Science (OCES), The Hong Kong University of Science and Technology (HKUST), Clear Water Bay, Kowloon, Hong Kong SAR, China

[3]Integrated Bioresource Information Division, BioResource Research Center, RIKEN, Tsukuba, Ibaraki 305-0074, Japan

[4]Faculty of Culture and Information Science, Doshisha University, Kyotanabe, Kyoto 610-0321, Japan

[5]School of Biological Sciences, The University of Queensland, St. Lucia, Brisbane, QLD 4072, Australia

[6]Department of International Health and Medical Anthropology, Institute of Tropical Medicine, Nagasaki University, Nagasaki 852-8523, Japan

[7]Institute for Chemical Research, Kyoto University, Gokasho, Uji, Kyoto 611-0011, Japan

[8]Faculty of Food and Agricultural Sciences, Fukushima University, Kanayagawa 1, Fukushima, Fukushima 960-1296, Japan.

[9]Institute for Advanced Biosciences, Keio University, Tsuruoka, Yamagata 997-0052, Japan.

[10]Gut Environmental Design Group, Kanagawa Institute of Industrial Science and Technology, Kawasaki, Kanagawa 210-0821, Japan.

[11]Transborder Medical Research Center, University of Tsukuba, Tsukuba, Ibaraki 305-8575,

Japan.

[12]Laboratory for Regenerative Microbiology, Juntendo University Graduate School of Medicine, Tokyo 113-8421, Japan.

[13]Department of Ecological Science, Vrije Universiteit Amsterdam, Amsterdam, the Netherlands

†**Correspondence:** Hiroaki Fujita (fujita.h@ecology.kyoto-u.ac.jp) or Hirokazu Toju (toju.hirokazu.4c@kyoto-u.ac.jp).

Abstract

Species utilizing the same resources often fail to coexist for extended periods of time. Such competitive exclusion mechanisms potentially underly microbiome dynamics, causing breakdowns of communities composed of species with similar genetic backgrounds of resource utilization. Although genes responsible for competitive exclusion among a small number of species have been investigated in pioneering studies, it remains a major challenge to integrate genomics and ecology for understanding stable coexistence in species-rich communities. Here, we show that community-scale analyses of functional gene redundancy can provide a useful platform for interpreting and predicting collapse of bacterial communities. Through 110-day time-series of experimental microbiome dynamics, we analyzed the metagenome-assembled genomes of co-occurring bacterial species. We then inferred ecological niche space based on the multivariate analysis of the genome compositions. The analysis allowed us to evaluate potential shifts in the level of niche overlap between species through time. We hypothesized that community-scale pressure of competitive exclusion could be evaluated by quantifying overlap of genetically determined resource-use profiles (metabolic pathway profiles) among coexisting species. We found that the degree of community compositional changes observed in the experimental microbiome was explained by the magnitude of gene-repertoire overlaps among bacterial species. The metagenome-based analysis of genetic potential for competitive exclusion will help us forecast major events in microbiome dynamics such as sudden community collapse (i.e., dysbiosis).

INTRODUCTION

Classic niche theory predicts that coexistence of species requires interspecific difference in resource use patterns [1–6]. Although some specific mechanisms can promote stable coexistence even with complete resource overlap (e.g., spatial structure of habitats and temporal variability in resource availability), similarity/dissimilarity in basic resource dependency among species is the basic factor determining the occurrence of competitive exclusion [7–9]. Therefore, evaluating the overlap of "fundamental niches", which are defined by species' fundamental resource requirements and resource-use capabilities [10, 11], is an essential step for understanding and predicting community-level dynamics.

Insights into fundamental niches are encrypted in species' genomes [12–14]: as species' traits are encoded in their DNA, genomic information provides the ultimate basis for evaluating target species' fundamental niches [15, 16]. Thus, potential strength of competitive interactions within ecological guilds or communities could be evaluated based on the distribution of species' gene repertoires within ecological niche space inferred with metagenomic data [12, 15, 16], also referred to as "metagenomic niche space". Although overlap of niches does not always cause competitive exclusion [7–9], higher levels of gene repertoire overlap within a community may impose greater impacts on population dynamics of constituent species.

In considering coexistence of microbial species, it is essential to examine whether such competition-driven population-level phenomena underly drastic ecological events observed at the community level. Microbial communities sometimes show sudden and substantial changes in species and/or taxonomic compositions [17–20]. Human gut microbiomes, for example, have been reported to show drastic shifts from species-rich states to "imbalanced" states with low α-diversity and overrepresentation of pathogenic species [21–24] (e.g., *Clostridium difficile*). Elucidating the ecological mechanisms causing such drastic community-level events provide fundamental insights into microbiome dynamics [24–26]. In this respect, an important challenge is to test the hypothesis that high levels of gene-repertoire overlap are observable prior to drastic community compositional changes. However, this hypothesis, to our knowledge, has not yet been tested presumably due to the paucity of time-series observations of microbiomes with substantial compositional changes. Even if such microbiome time-series data are available, analyses of potential niche (gene repertoire) overlap require another line of information. Specifically, we need data of respective species' genomes at multiple time points. Therefore, developing research systems that can overcome these constrains will deepen our understanding of microbiome ecological processes.

In this study, we test the degree to which gene-repertoire overlap changes through dynamics of species-rich microbial communities. By targeting an experimental microbial system showing rapid and substantial changes in taxonomic compositions [19], we infer niche space depicting species' gene repertoires. Work in this system using a metabolic modeling analysis demonstrated that interactions between species were keys to understand the drastic microbiome dynamics [27]. Now, by compiling the shotgun metagenomic data collected at 13 time points across the 110-day time-series of the experiment, we reveal temporal shifts in the magnitude of gene repertoire overlap among microbial species. We then examine whether a

high level of fundamental-niche overlap is observed prior to drastic changes in community structure. Overall, we explore how signs of drastic shifts in community structure are detected by inferring community-scale degree of fundamental niche overlap with the aid of genomic information.

RESULTS

Functional dynamics of microbiomes

We focused on the experimental microbiome showing drastic shifts in taxonomic compositions [19]. In a previous study [19], a 110-day monitoring of microbiomes was performed with six experimental settings. To set up experimental microbiomes with high diversity of bacterial species/taxa, we used natural microbial communities derived from soil or pond-water ecosystems as source inocula, rather than "synthetic" communities with pre-defined diversity. Specifically, microbiomes were set up with combinations of two source inoculum types (soil- or pond-water-derived inoculum microbiomes) and three medium types (oatmeal, oatmeal-peptone, or peptone broth medium) with eight replications ($2 \times 3 \times 8 = 48$ microbiomes; see Materials and Methods for details). From each of the 48 microbiomes, a fraction of each replicate community was sampled every 24 hours. The collected samples were subjected to the amplicon sequencing of the 16S rRNA region and the temporal changes in community compositions were monitored throughout the time-series [19]. By calculating the magnitude of time-series changes in community compositions [19] (Fig. 1A), we focused on a water-inoculum/oatmeal-medium replicate community showing the most abrupt (rapid and substantial) changes in community compositions among the 48 microbiomes examined as described in a study on metabolic interactions between species [27] (Fig. S1).

By targeting the replicate community mentioned above, we compiled shotgun metagenomic data at 13 time points across the time-series [27]. In total, 32 high-quality (> 80 % completeness and < 5 % contamination) metagenome-assembled genomes (MAGs) belonging to 20 genera (16 families; 12 orders) were detected [27] (Figs. 1B-C and 2; Fig. S2; Table S1). As indicated in the amplicon sequencing analysis [19] (Fig. 1A), drastic shifts from taxon-rich community states to oligopolistic states was observed around Day 20 in the shotgun sequencing analysis (Fig. 1B).

After the drastic community compositional change, the system reached a quasi-stable state represented by the dominance of a *Hydrotalea* (Chitinophagaceae) bacterium (Fig. 1B).

The MAG of the *Hydrotalea* was characterized by relatively low GC content (38 %) and relatively small genome size within the community (ca. 3.1 Mb; Fig. 2A). In contrast, the two bacterial MAGs consistently coexisted with the dominant *Hydrotalea* through the time-series (i.e., *Terracidiphilus* and *Mangrovibacter*) had larger genome size (4.2 and 5.4 Mb, respectively; Fig. 1C), characterized by various genes absent from the *Hydrotalea* genome (Fig. 2; Fig. S3). Specifically, the *Terracidiphilus* MAG showed metabolic pathways/processes for degrading plant-derived biopolymers (e.g., cellulose; Fig. 2), potentially surviving as a primary user of polymer compounds within the plant-derived (oatmeal) medium. Meanwhile, the *Mangrovibacter* MAG had pathways/processes related to starch degradation (e.g., amylase) and vitamin-B_{12} transportation, which were absent from the genomes of *Hydrotalea, Terracidiphilus*, and the other MAG (*Rhizomicrobium*) detected on Day 40-60 (Fig. 2).

Multivariate analysis of gene repertoires

Next, we used the shotgun metagenomic data to evaluate how the level of gene repertoire overlap among microbes shifted through time. We anticipated that microbial species with similar resource-use abilities or restrictions have similar genomic structure. Therefore, it is expected that species competing for the same resource tend to form clusters within the space defined based on the principal coordinate analysis (PCoA) of dissimilarity in gene repertoires. For each pair of the 32 MAGs, dissimilarity (Jaccard distance) of gene repertoires was calculated based on the matrix representing the presence/absence of the 6,999 genes annotated with the program Prokka [28]. A PCoA was then performed using the β-diversity information (Fig. 3A). At each of the 13 time points, detected MAGs were plotted on the PCoA space. Since we did not have *a priori* knowledge of specific metabolic pathways keys to the microbe-to-microbe competition within the experimental microbiome, all datasets were included in this multivariate analysis. Given general characteristics of multivariate analysis based on β-diversity metrics, the multivariate reconstruction of ecological niche space depends greatly on the genes whose presence/absence profiles vary among species, while housekeeping genes possessed by most species are expected to contribute little to the multivariate analysis.

We found that alphaproteobacterial and gammaproteobacterial MAGs respectively constituted some clusters within the niche space reconstructed based on the multivariate

163 analysis early in the microbiome dynamics (Day 1-20; Fig. 3B). This state with high niche
164 overlap and potential within-guild competition for resources then collapsed into a simpler
165 community state represented by *Hydrotalea*, *Mangrovibacter*, *Terracidiphilus*, and
166 *Rhizomicrobium* as detailed above (Fig. 3B). The space once occupied by many
167 alphaproteobacterial and gammaproteobacterial MAGs remained unoccupied or sparsely
168 occupied after the community compositional collapse. Even when the number of MAGs
169 detectable with our shotgun-metagenomic sequencing increased again late in the time-series,
170 dense aggregations of microbes with similar genomic compositions remained unobserved
171 (Fig. 3B).

172

173 **Metagenomic niche overlap**

174 We next quantitatively evaluated dynamics in the magnitude of community-scale niche
175 overlap within the multivariate space (Fig. 3). We developed two types of simple indices for
176 evaluating community-scale niche overlap. The one is defined as the overall mean of gene-
177 repertoire similarity between pairs of MAGs within a community. For a time point, the niche
178 overlap index is calculated as:

179 $$\text{niche overlap score (overall mean)} = 1 - \frac{\sum_{i \in T, j \in T, i \neq j} D_{ij}}{N_T(N_T - 1)},$$

180 where T is the set of MAGs detected on a focal day (relative abundance > 0.1 %), D_{ij} is the
181 Jaccard metric of dissimilarity [29] in gene compositions, and N_T is the number of MAGs
182 detected on the day. By definition, this niche overlap value based on Jaccard dissimilarity
183 varies from 0 (completely different repertoires of genes in all pairs of MAGs) and 1
184 (completely identical gene repertoires in all pairs of MAGs), allowing us to evaluate niche
185 overlap levels of target communities within the standardized ranges. The other index is
186 defined as mean value of gene-repertoire similarity with nearest neighbors. The alternative is
187 calculated as:

188 $$\text{niche overlap score (nearest mean)} = 1 - \frac{\sum_{i \in T, i \neq j} \min_{j \in T}(D_{ij})}{N_T}.$$

189 This index can be modified by incorporating the information of the relative abundance of
190 MAGs (p_i) as follows:

$$\text{niche overlap score (weighted nearest mean)} = 1 - \sum_{i \in T, i \neq j} p_i \min_{j \in T}(D_{ij}).$$

The results indicated that the level of niche overlap was the highest on Day 1 or Day 10 and that it decreased until Day 30 (Fig. 4A). Although the niche overlap score remained low between Day 40 and 60, it increased again late in the microbiome time-series (Fig. 4B). Note that α-diversity of the community showed similar temporal shifts and it was significantly associated with the niche overlap indices (Fig. 4B-C). Through the time-series, the estimated niche overlap level was significantly associated with the magnitude of the observed community compositional changes (Fig. 5)

DISCUSSION

By developing simple metrics of among-species overlap of gene repertoires, we examined potential relationship between community-scale niche overlap and drastic changes in community structure. Early in the experimental microbiome dynamics, alphaproteobacterial and gammaproteobacterial species were present, resulting in relatively high niche-overlap scores at the community level (Figs. 3 and 4). The quasi-equilibrium state of microbial compositions then collapsed into another quasi-equilibrium represented by a small number of bacteria varying in genome size and metabolic capabilities. Throughout the time-series, higher niche overlap levels entailed greater changes in microbial community compositions (Fig. 5). These findings lead to the working hypothesis that collapse of microbiome structure is predicted by the level of potential niche overlap within multivariate metagenomic space. In light of the "limiting similarity" rule of ecological niches [30], microbial species that exceed a critical limit of genome compositional similarity are expected to compete for the same resources intensively, eventually driving competitive exclusion processes. Thus, as examined in this study, similarity/dissimilarity in genetically determined resource-use properties (i.e., fundamental niches) sets baselines for consequences of interspecific interactions.

The results also indicated that niche overlap level does not necessarily show monotonic decrease through microbial community processes. Although gene-repertoire overlap level and detectable species richness sharply declined early in the microbiome dynamics, both variables gradually increased again around Day 80 (Figs. 1A and 4B). In the resurgence process, however, the dense clusters of alphaproteobacterial or gammaproteobacterial species detected until Day 20 did not appear again within the niche space (Fig. 3B). These observations

222 suggest that once collapsed, microbial communities may not return to previous states with
223 highest levels of niche overlap, but refilling of poorly-used niches can occur under the
224 constraint of limiting similarity within niche space. Although these insights are useful, our
225 present analysis is based only on 13 time points of a microbiome experiment. Due to the
226 limitation, it remained difficult to separate effects of α-diversity from those of gene-repertoire
227 overlap (Fig. 4B-C). Thus, the statistical analysis proposed in this study need to be expanded
228 by reducing the cost of metagenomic sequencing as well as by developing more efficient
229 pipelines for the computationally intensive analyses of metagenomic datasets.

230 The approach of systematically evaluating potential overlap of ecological niches have
231 been previously explored in "community phylogenetics", in which phylogenetic
232 overdispersion/clustering is evaluated based on null model analysis of random assembly from
233 species pools [5, 31, 32]. In those studies based on phylogenetic analyses, similarity of niches
234 has been inferred based on the assumption that phylogenetically similar species have similar
235 ecological properties (e.g., resource requirements). Nonetheless, given that convergent
236 evolution of ecologically important traits is ubiquitous in the history of life [33–35], the
237 assumption of phylogenetic niche conservatism is not always met [36]. Therefore, because
238 gene repertoires are more direct proxies of species traits than phylogeny, metagenome-based
239 analyses will deepen our understanding of community processes driven by competitive
240 exclusion. Meanwhile, in the present analyses of gene repertoire overlap, we included whole
241 metagenomic datasets of the examined microbes due to the lack of *a priori* insights into the
242 metabolic pathways/processes playing essential roles in interspecific competition for
243 resources. In this respect, our analysis is a preliminary conceptual step for evaluating potential
244 overlap of fundamental niches at the community level. In future studies, analyses excluding
245 housekeeping genes [37, 38] or those focusing on specific functional groups of genes (e.g.,
246 carbohydrate degrading genes [39]) may provide more reliable inference of niche overlap.
247 Because such selection of genes can critically influence threshold niche-overlap values for
248 anticipating abrupt community compositional changes, setting a commonly applicable
249 criterion of choosing target gene sets will help us perform comparative analyses across a wide
250 range of microbial communities.

251 The simple framework for evaluating overlap of fundamental niches is applicable to
252 diverse types of microbiomes. Given that our Jaccard-dissimilarity-based indices are
253 standardized within the range from 0 to 1, the next crucial step is to examine how threshold
254 niche overlap values for anticipating microbial community collapse vary among different

types of ecosystems. Such threshold values can vary among ecosystems depending on their basic levels of sustainable functional redundancy. In our laboratory microbiome, for example, the lack of spatial structure (e.g., refuges for inferior species) and environmental fluctuations (e.g., temperature fluctuations) might have severely limited coexistence of functionally similar species (species with similar metabolic capabilities). In contrast, in human gut microbiomes, spatial complexity [40, 41] and temporally fluctuating environmental conditions [22] may reduce the risk of competitive exclusion, allowing higher levels of niche overlap within communities. Thus, extension of time-series metagenomic analyses to diverse types of ecosystems [42–45] will enhance our knowledge of relationship among ecosystem properties, functional redundancy, and community stability.

While genomic information provides an ultimate platform for inferring fundamental niches [12–14], overlap of gene repertoires may not always result in competitive exclusion of species within communities. Even in a pair of species with similar gene repertoires, differentiation in gene expression patterns may occur to avoid overlap of resource-use patterns between species, allowing coexistence of the two species in an environment. Such differentiation of "realized niches [10]" through phenotypic plasticity is potentially evaluated by transcriptomic or metabolomic analyses [46, 47]. Consequently, integration of (meta)transcriptome and (meta)metabolome analyses [48–50] with metagenome-based analyses will reorganize our understanding of deterministic processes in microbiome dynamics.

MATERIALS AND METHODS

Time-series data of experimental microbiomes

We used the experimental system of the microbiome time-series monitoring described in a previous study [19]. In the experiment, microbiomes differing in the magnitude of community compositional shifts were constructed across the six treatments defined by the combinations of two inoculum sources and three types of media. One of the source microbiomes derived from the soil collected from the A layer (0-10 cm in depth) in the research forest of Center for Ecological Research, Kyoto University, Otsu, Japan (34.972 ºN; 135.958 ºE). The other source inoculum was prepared by collecting water from a pond ("Shoubuike") near Center for Ecological Research (34.974 ºN, 135.966 ºE). Each of the source inocula was introduced into oatmeal (Medium-A), oatmeal-peptone (Medium-B), or peptone (Medium-C) broth media with eight replicates. Thus, in total, 48 experimental microcosms (two source microbiomes × three media × eight replicates) were constructed in a deep-well plate (1000-µL-scale culture in each well). The plate was kept shaken at 1,000 rpm at 23 ºC. After five-day pre-incubation, 200 µL out of the 1,000-µL culture medium was sampled from each well every 24 hours for 110 days. In each sampling event, 200 µL of fresh medium was added to each well so that the total culture volume was kept constant. In total, 5,280 samples (48 communities/day × 110 days) were collected through the time-series experiment. After DNA extraction, the samples were subjected to the amplicon sequencing analysis of the 16S rRNA region [19]. To quantify the speed and magnitude of community shifts through time, the "abruptness" index was calculated through the time-series of each replicate microcosm in each experimental treatment [19]. Specifically, an estimate of the abruptness index for time point t was obtained as the Bray-Curtis β-diversity between average community compositions from time points $t - 4$ to t and those from $t + 1$ to $t + 5$ (i.e., dissimilarity between 5-day time-windows). The Bray-Curtis β-diversity [51] was calculated as $\frac{\sum_{i=1}^{n}|X_{ij}-X_{ik}|}{\sum_{i=1}^{n}(X_{ij}+X_{ik})}$, where X_{ij} and X_{ik} denoted relative abundance of microbial amplicon sequence variant (ASV) i in the compared time windows (j, from $t - 4$ to t; k, from $t + 1$ to $t + 5$). An abruptness score larger than 0.5 indicates that turnover of more than 50 % of community compositions occurred between the time-windows [19].

Shotgun metagenomics

Focusing on a replicate microcosm in which the most rapid and substantial turnover of community compositions was observed (replicate no. 5 of Water/Medium-A treatment; Fig. S1), shotgun metagenomic sequencing was conducted by targeting 13 samples (Day 1, 10, 20, 24, 30, 40, 50, 60, 70, 80, 90, 100, and 110) as described elsewhere [27]. Specifically, each DNA sample was processed with Nextera XT DNA Library Preparation Kit (Illumina) and sequenced with the DNBSEQ-G400 (BGI; 200-bp paired-end sequencing). From the output data, sequencing adaptors were removed using Cutadapt [52] 2.5 and quality filtering was performed with Fastp [53] 0.21.0: ca. 10 Gb/sample was subjected to the analysis [in total, 159.96 Gb (1000.301 M reads)]. The sequences of each sample were assembled with metaSPAdes [54] 3.15.2. Binning was then performed with MetaWRAP [55] 1.3.2, followed by quality assessing with CheckM [56] 1.1.3. The identity between MAGs were calculated using FastANI [57] 1.33 and MAGs with > 99 % identity were dereplicated through the time-series (Table S1). In the dereplication, the MAGs with the highest completeness and N50 statistics were selected as representative MAGs. Read-coverage was then calculated with CoverM [58] 0.6.0, followed by taxonomic annotation was performed using GTDB-Tk [59, 60] 1.6. Only the MAGs with > 80 % completeness and < 5 % contamination were used in the downstream analyses. Gene annotation was performed with Prokka [28] 1.14.6, yielding 6,999 annotated genes (Data S1). To conduct additional functional annotation of genes, the orthology numbers of Kyoto Encyclopedia of Genomes (KEGG) were retrieved using GhostKOALA [61] 2.2. For respective microbial MAGs (bins), completeness of metabolic pathways was estimated with KEGG decoder [62] 1.3. Based on the matrix representing KEGG metabolic pathway/process profiles of respective MAGs (Data S2), a heatmap showing pathway/process completeness was drawn (Fig. S3).

Background environmental conditions

For the 13 samples subjected to the shotgun metagenomic analysis, concentrations of ammonium (NH_4^+) and nitrate (NO_3^-) were measured to obtain supplementary information of background environmental conditions. Colorimetric methods with a modified indophenol reaction [63, 64] and the VCl3/Griess assay were applied for the measurements of NH_4^+ and NO_3^-, respectively. Samples were run in triplicates via a standard addition method to account for individual matrix effects [65].

Multivariate analysis of the metagenomic space

Based on the whole matrix representing the profiles of the 6,999 genes (Data S1), the Jaccard metric of distance was calculated for each pair of the 32 microbial MAGs (D_{ij}, where i and j represent MAGs). The Jaccard-distance estimates were then used to perform a principal coordinate analysis (PCoA). Using the obtained principal coordinate scores, all the microbial MAGs detected through the time-series were plotted on a multivariate space consisting of the first three PCoA axes (PCoA 1, PCoA 2, and PCoA 3). At each time point, the MAGs detected with the shotgun metagenomic sequencing (defined as the MAGs whose relative abundance is greater than 0.1 %) was plotted on the three-dimensional space defined with the PCoA axes.

Evaluation of niche overlap level

The community-scale magnitude of potential niche overlap among species was evaluated based on the shogun metagenomic sequencing dataset. We developed two types of simple indices for evaluating community-scale niche overlap as detailed in the Results section. To test whether a high level of fundamental-niche overlap is observed prior to drastic changes in microbial community structure, we examined relationship between the above niche overlap index and time-series shifts in community structure (Bray-Curtis β-diversity between present and next time points through the time-series of the shotgun metagenomic data).

REFERENCES

1. Gause GF. The Struggle for Coexistence. 1934. Williams & Wilkins, Baltimore.

2. Hardin G. The competitive exclusion principle. *Science (1979)* 1960; **131**: 1292–1297.

3. Volterra V. Variations and fluctuations of the number of individuals in animal species living together. *ICES Journal of Marine Science* 1928; **3**: 3–51.

4. Zaret TM, Rand AS. Competition in tropical stream fishes: support for the competitive exclusion principle. *Ecology* 1971; **52**: 336–342.

5. Mayfield MM, Levine JM. Opposing effects of competitive exclusion on the phylogenetic structure of communities. *Ecol Lett* 2010; **13**: 1085–1093.

6. Grime JP. Competitive exclusion in herbaceous vegetation. *Nature* 1973; **242**: 344–347.

7. Letten AD, Ke PJ, Fukami T. Linking modern coexistence theory and contemporary niche theory. *Ecol Monogr* 2017; **87**: 161–177.

8. Chesson P. Updates on mechanisms of maintenance of species diversity. *Journal of Ecology* 2018; **106**: 1773–1794.

9. Chesson P. Mechanisms of maintenance of species diversity. *Annu Rev Ecol Syst* 2000; **31**: 343–366.

10. Chase JM, Leibold MA. Ecological niches: linking classical and contemporary approaches. *Biodiversity and Conservation* . 2004. University of Chicago Press, Chicago.

11. Hutchinson GE. Concluding Remarks. *Cold Spring Harb Symp Quant Biol* 1957; **22**: 415–427.

12. Régimbeau A, Budinich M, Larhlimi A, Pierella Karlusich JJ, Aumont O, Memery L, et al. Contribution of genome-scale metabolic modelling to niche theory. *Ecol Lett* 2022; **25**: 1352–1364.

13. Smith SR, Dupont CL, McCarthy JK, Broddrick JT, Oborník M, Horák A, et al. Evolution and regulation of nitrogen flux through compartmentalized metabolic networks in a marine diatom. *Nat Commun* 2019; **10**: 4552.

14. Palomo A, Pedersen AG, Fowler SJ, Dechesne A, Sicheritz-Pontén T, Smets BF. Comparative genomics sheds light on niche differentiation and the evolutionary history of comammox *Nitrospira*. *ISME Journal* 2018; **12**: 1779–1793.

15. Alneberg J, Bennke C, Beier S, Bunse C, Quince C, Ininbergs K, et al. Ecosystem-wide metagenomic binning enables prediction of ecological niches from genomes. *Commun Biol* 2020; **3**: 1–10.

16. Fahimipour AK, Gross T. Mapping the bacterial metabolic niche space. *Nat Commun* 2020; **11**: 1–8.

17. Carding S, Verbeke K, Vipond DT, Corfe BM, Owen LJ. Dysbiosis of the gut microbiota in disease. *Microb Ecol Health Dis* 2015; **26**: 26191.

18. Ravel J, Brotman RM, Gajer P, Ma B, Nandy M, Fadrosh DW, et al. Daily temporal dynamics of vaginal microbiota before, during and after episodes of bacterial vaginosis. *Microbiome* 2013; **1**: 29.

19. Fujita H, Ushio M, Suzuki K, Abe M, Yamamichi M, Iwayama K, et al. Alternative stable states, nonlinear behavior, and predictability of microbiome dynamics. *Microbiome* 2023; **11**: 63.

20. Yajima D, Fujita H, Hayashi I, Shima G, Suzuki K, Toju H. Core species and interactions prominent in fish-associated microbiome dynamics. *Microbiome* 2023; **11**: 53.

21. Lahti L, Salojärvi J, Salonen A, Scheffer M, de Vos WM. Tipping elements in the human intestinal ecosystem. *Nat Commun* 2014; **5**: 4344.

22. David LA, Maurice CF, Carmody RN, Gootenberg DB, Button JE, Wolfe BE, et al. Diet rapidly and reproducibly alters the human gut microbiome. *Nature* 2014; **505**: 559–563.

23. Kho ZY, Lal SK. The human gut microbiome - A potential controller of wellness and disease. *Front Microbiol* 2018; **9**: 1835.

24. Kriss M, Hazleton KZ, Nusbacher NM, Martin CG, Lozupone CA. Low diversity gut microbiota dysbiosis: drivers, functional implications and recovery. *Curr Opin Microbiol* 2018; **44**: 34–40.

25. Costello EK, Stagaman K, Dethlefsen L, Bohannan BJM, Relman DA. The application of ecological theory toward an understanding of the human microbiome. *Science (1979)* 2012; **336**: 1255–1262.

26. Huttenhower C, Gevers D, Knight R, Abubucker S, Badger JH, Chinwalla AT, et al. Structure, function and diversity of the healthy human microbiome. *Nature* 2012; **486**: 207–214.

27. Fujita H, Ushio M, Suzuki K, Abe MS, Yamamichi M, Okazaki Y, et al. Facilitative interaction networks in experimental microbial community dynamics. *Front Microbiol* . 2023. , **14**: 1153952

28. Seemann T. Prokka: Rapid prokaryotic genome annotation. *Bioinformatics* 2014; **30**:

2068–2069.

29. Anderson MJ, Crist TO, Chase JM, Vellend M, Inouye BD, Freestone AL, et al. Navigating the multiple meanings of β diversity: A roadmap for the practicing ecologist. *Ecol Lett* 2011; **14**: 19–28.

30. Macarthur R, Levins R. The limiting similarity, convergence, and divergence of coexisting species. *American Naturalist* 1967; **101**: 377–385.

31. Webb CO, Ackerly DD, McPeek MA, Donoghue MJ. Phylogenies and community ecology. *Annu Rev Ecol Syst* 2002; **33**: 475–505.

32. Cavender-Bares J, Kozak KH, Fine PVA, Kembel SW. The merging of community ecology and phylogenetic biology. *Ecol Lett* 2009; **12**: 693–715.

33. Marvig RL, Sommer LM, Molin S, Johansen HK. Convergent evolution and adaptation of Pseudomonas aeruginosa within patients with cystic fibrosis. *Nat Genet* 2015; **47**: 57–64.

34. McCutcheon JP, McDonald BR, Moran NA. Convergent evolution of metabolic roles in bacterial co-symbionts of insects. *Proc Natl Acad Sci U S A* 2009; **106**: 15394–15399.

35. Merhej V, Royer-Carenzi M, Pontarotti P, Raoult D. Massive comparative genomic analysis reveals convergent evolution of specialized bacteria. *Biol Direct* 2009; **4**: 13.

36. Losos JB. Phylogenetic niche conservatism, phylogenetic signal and the relationship between phylogenetic relatedness and ecological similarity among species. *Ecol Lett* . 2008. , **11**: 995–1007

37. Gibson DG, Glass JI, Lartigue C, Noskov VN, Chuang R-Y, Algire M a, et al. Creation of a bacterial cell controlled by a chemically synthesized genome. *Science* 2010; **329**: 52–6.

38. Maiden MCJ, van Rensburg MJJ, Bray JE, Earle SG, Ford SA, Jolley KA, et al. MLST revisited: The gene-by-gene approach to bacterial genomics. *Nat Rev Microbiol* 2013; **11**: 728–736.

39. Flint HJ, Scott KP, Duncan SH, Louis P, Forano E. Microbial degradation of complex carbohydrates in the gut. *Gut Microbes* 2012; **3**: 289–306.

455 40. Tropini C, Earle KA, Huang KC, Sonnenburg JL. The Gut Microbiome: Connecting
456 Spatial Organization to Function. *Cell Host Microbe* 2017; **21**: 433–442.

457 41. Earle KA, Billings G, Sigal M, Lichtman JS, Hansson GC, Elias JE, et al. Quantitative
458 Imaging of Gut Microbiota Spatial Organization. *Cell Host Microbe* 2015; **18**: 478–
459 488.

460 42. Jansson JK, Hofmockel KS. Soil microbiomes and climate change. *Nat Rev Microbiol* .
461 2020. , **18**: 35–46

462 43. Fierer N. Embracing the unknown: Disentangling the complexities of the soil
463 microbiome. *Nat Rev Microbiol* 2017; **15**: 579–590.

464 44. Trivedi P, Leach JE, Tringe SG, Sa T, Singh BK. Plant–microbiome interactions: from
465 community assembly to plant health. *Nat Rev Microbiol* 2020; **18**: 607–621.

466 45. Venter JC, Remington K, Heidelberg JF, Halpern AL, Rusch D, Eisen JA, et al.
467 Environmental Genome Shotgun Sequencing of the Sargasso Sea. *Science (1979)*
468 2004; **304**: 66–74.

469 46. Nowinski B, Moran MA. Niche dimensions of a marine bacterium are identified using
470 invasion studies in coastal seawater. *Nat Microbiol* 2021; **6**: 524–532.

471 47. Pereira FC, Berry D. Microbial nutrient niches in the gut. *Environ Microbiol* 2017; **19**:
472 1366–1378.

473 48. Heintz-Buschart A, Wilmes P. Human gut microbiome: function matters. *Trends*
474 *Microbiol* 2018; **26**: 563–574.

475 49. Schirmer M, Franzosa EA, Lloyd-Price J, McIver LJ, Schwager R, Poon TW, et al.
476 Dynamics of metatranscription in the inflammatory bowel disease gut microbiome. *Nat*
477 *Microbiol* 2018; **3**: 337–346.

478 50. Turner TR, Ramakrishnan K, Walshaw J, Heavens D, Alston M, Swarbreck D, et al.
479 Comparative metatranscriptomics reveals kingdom level changes in the rhizosphere
480 microbiome of plants. *ISME Journal* 2013; **7**: 2248–2258.

481 51. Legendre P, de Cáceres M. Beta diversity as the variance of community data:
482 Dissimilarity coefficients and partitioning. *Ecol Lett* 2013; **16**: 951–963.

483 52. Martin M. Cutadapt removes adapter sequences from high-throughput sequencing
484 reads. *EMBnet J* 2011; **17**: https://doi.org/10.14806/ej.17.1.200.

485 53. Chen S, Zhou Y, Chen Y, Gu J. Fastp: An ultra-fast all-in-one FASTQ preprocessor.
486 *Bioinformatics* 2018; **34**: i884–i890.

487 54. Bankevich A, Nurk S, Antipov D, Gurevich AA, Dvorkin M, Kulikov AS, et al.
488 SPAdes: A new genome assembly algorithm and its applications to single-cell
489 sequencing. *Journal of Computational Biology* 2012; **19**: 455–477.

490 55. Uritskiy G v., DiRuggiero J, Taylor J. MetaWRAP—a flexible pipeline for genome-
491 resolved metagenomic data analysis. *Microbiome* 2018; **6**: 158.

492 56. Parks DH, Imelfort M, Skennerton CT, Hugenholtz P, Tyson GW. CheckM: Assessing
493 the quality of microbial genomes recovered from isolates, single cells, and
494 metagenomes. *Genome Res* 2015; **25**: 1043–1055.

495 57. Jain C, Rodriguez-R LM, Phillippy AM, Konstantinidis KT, Aluru S. High throughput
496 ANI analysis of 90K prokaryotic genomes reveals clear species boundaries. *Nat*
497 *Commun* 2018; **9**: 5114.

498 58. Woodcroft B. CoverM: program available at https://github.com/wwood/CoverM. 2021.

499 59. Chaumeil PA, Mussig AJ, Hugenholtz P, Parks DH. GTDB-Tk: A toolkit to classify
500 genomes with the genome taxonomy database. *Bioinformatics* 2020; **36**: 1925–1927.

501 60. Parks DH, Chuvochina M, Rinke C, Mussig AJ, Chaumeil P-A, Hugenholtz P. GTDB:
502 an ongoing census of bacterial and archaeal diversity through a phylogenetically
503 consistent, rank normalized and complete genome-based taxonomy. *Nucleic Acids Res*
504 2022; **50**: D785–D794.

505 61. Kanehisa M, Sato Y, Morishima K. BlastKOALA and GhostKOALA: KEGG Tools for
506 Functional Characterization of Genome and Metagenome Sequences. *J Mol Biol* 2016;
507 **428**: 726–731.

508 62. Graham ED, Heidelberg JF, Tully BJ. Potential for primary productivity in a globally-
509 distributed bacterial phototroph. *ISME Journal* 2018; **12**: 1861–1866.

510 63. Kandeler E, Gerber H. Short-term assay of soil urease activity using colorimetric
511 determination of ammonium. *Biol Fertil Soils* 1988; **6**: 68–72.

512 64. Hood-Nowotny R, Umana NH-N, Inselbacher E, Oswald- Lachouani P, Wanek W.
513 Alternative methods for measuring inorganic, organic, and total dissolved nitrogen in
514 soil. *Soil Science Society of America Journal* 2010; **74**: 1018–1027.

515 65. Taylor BW, Keep CF, Hall RO, Koch BJ, Tronstad LM, Flecker AS, et al. Improving
516 the fluorometric ammonium method: Matrix effects, background fluorescence, and
517 standard additions. *J North Am Benthol Soc* 2007; **26**: 167–177.

518

ACKNOWLEDGEMENTS

Computation time was provided by the SuperComputer System, Institute for Chemical Research, Kyoto University. This work was financially supported by JST PRESTO (JPMJPR16Q6), Human Frontier Science Program (RGP0029/2019), JSPS Grant-in-Aid for Scientific Research (20K20586), NEDO Moonshot Research and Development Program (JPNP18016), and JST FOREST (JPMJFR2048) to H.T., JSPS Grant-in-Aid for Scientific Research (20K06820 and 20H03010) to K.S., and JSPS Fellowship to H.F. and A.C.

AUTHOR CONTRIBUTIONS

H.T. designed the work with H.F. H.F. and A.C. performed experiments. H.F. analyzed the data with Y.O., and H.T. H.F. and H.T. wrote the paper with all the authors.

COMPETING INTERESTS

The authors declare no competing interests.

DATA AVAILABILITY STATEMENT

The 16S rRNA sequencing data reported in a previous study [19] are available from the DNA Data Bank of Japan (DDBJ) with the accession number DRA013352, DRA013353, DRA013354, DRA013355, DRA013356, DRA013368 and DRA013379. The shotgun metagenomic data reported previous [27] are available with the DDBJ accession number DRA013382. The microbial community data are deposited at our GitHub repository (https://github.com/hiroakif93/MTS_nicheSpace) [to be publicly available after acceptance of the paper]. The matrices of the shotgun metagenomic data are available as Data S1 and 2. All the scripts used to analyze the data are available at the GitHub repository (https://github.com/hiroakif93/MTS_nicheSpace) [to be publicly available after acceptance of the paper].

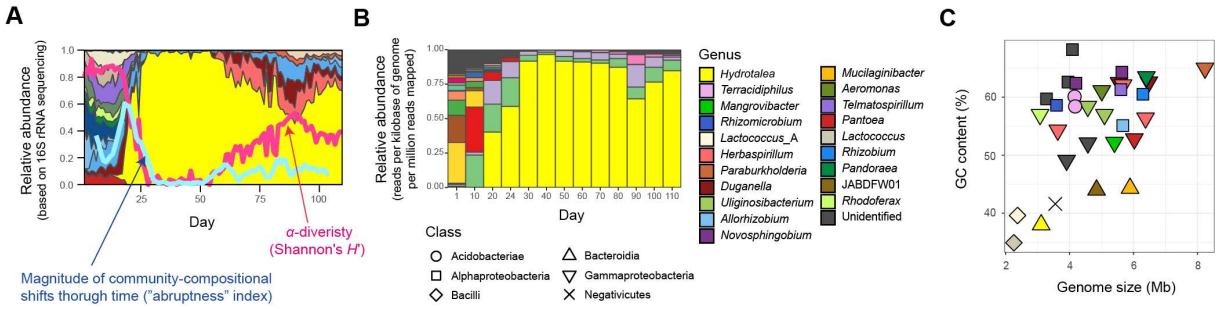

546

547 **Fig. 1 Community and ecosystem dynamics. A** Time-series data of community structure.
548 For the replicate microcosm that showed the most abrupt community compositional changes
549 through the 110-day microbiome experiment [19] (Fig. S1), family-level taxonomic
550 compositions inferred with 16S rRNA sequencing are shown. The blue line represents the
551 speed and magnitude of community compositional changes around each time point
552 ("abruptness" index [19]; see Materials and Methods). The red line indicates α-diversity
553 (Shannon's *H'*) of microbial ASVs [19]. Note that a value larger than 0.5 represents turnover
554 of more than 50 % of microbial ASV compositions. See Fig. S1 for color profiles of bacterial
555 families. Reproduced from the data of a previous study [19]. **B** Taxonomic compositions
556 inferred with shotgun metagenomic sequencing. At each of the 13 time points through the
557 time-series of the target microcosm, the relative abundance of each MAG was estimated
558 based on the normalized read coverage value (reads per kilobase of genome per million reads
559 mapped). **C** Genome size and GC nucleotide content of the MAGs detected in the target
560 microcosm. See panel **A** for colors and symbols.
561

562

563 **Fig. 2 Metabolic pathway/process profiles of the MAGs.** KEGG metabolic
564 pathways/profiles of the reconstructed bacterial genomes (MAGs) are shown. The detection
565 (relative abundance > 0.1 %) of each microbial MAG on each day within the shotgun
566 metagenomic data is indicated in the panel below. Only the microbial MAGs with > 80 %
567 completeness and < 5 % contamination were included (Table S1). The five MAGs that co-
568 occurred from Day 40 to 60 and metabolic pathways/processes mentioned in the main text are
569 highlighted. Only the metabolic pathways/processes with highly heterogeneous patterns
570 across microbial MAGs are shown. See Fig. S3 for detailed profiles of the metabolic

571 pathways/processes.

572

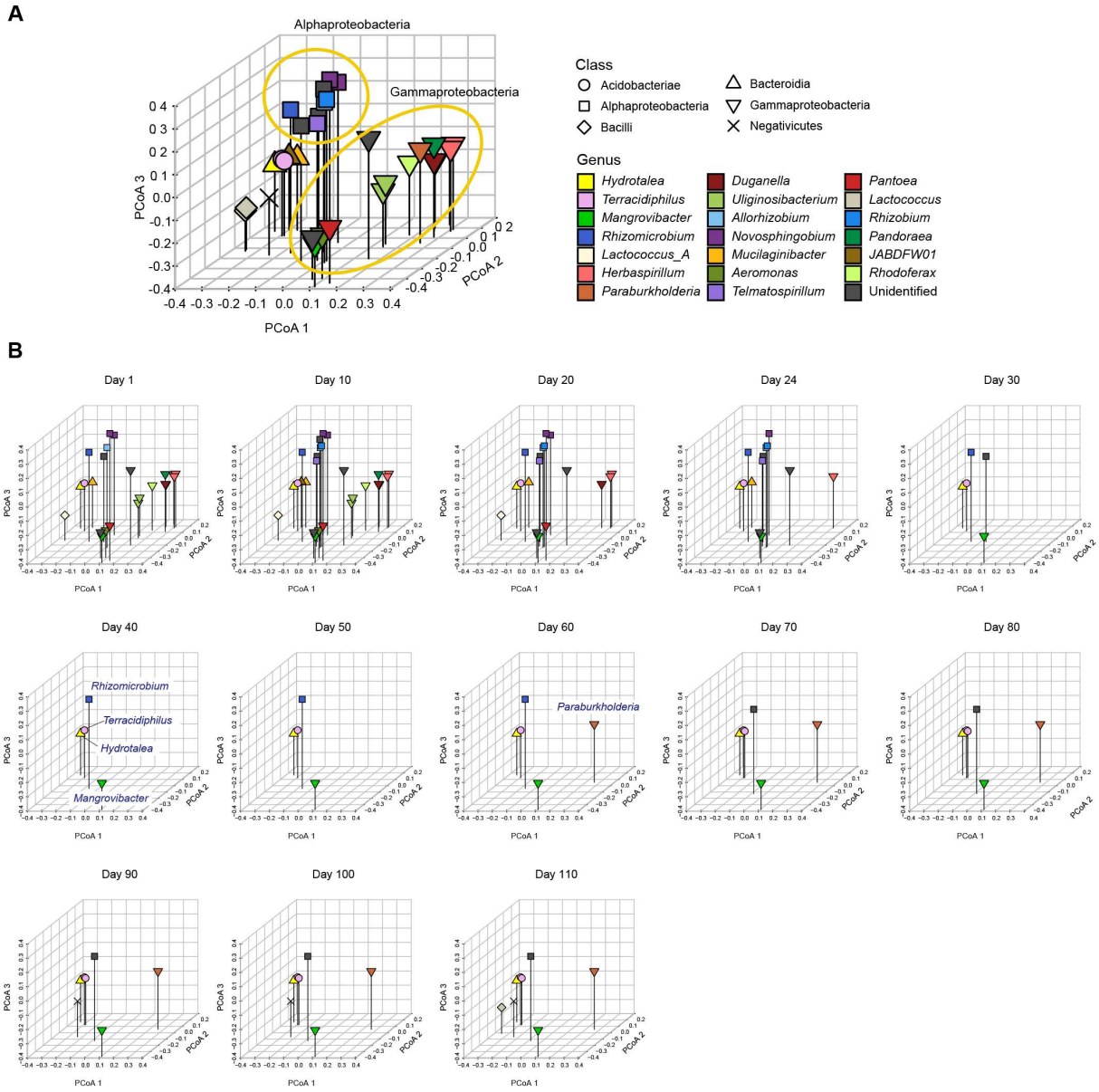

573

574 **Fig. 3 Metagenomic niche space**. **A** Distributions of MAGs within metagenomic niche
575 space. Based on dissimilarity in gene repertoires, microbial MAGs that appeared in the time-
576 series of the target microcosm were plotted on the three-dimensional space defined by the
577 principal coordinate analysis (PCoA) of 6,999 genes. **B** Changes in the distributions of
578 microbial MAGs within niche space. At each time point, detected MAGs (relative abundance
579 > 0.1 %) were plotted on the space defined in the multivariate analysis in the in the panel **A**.
580

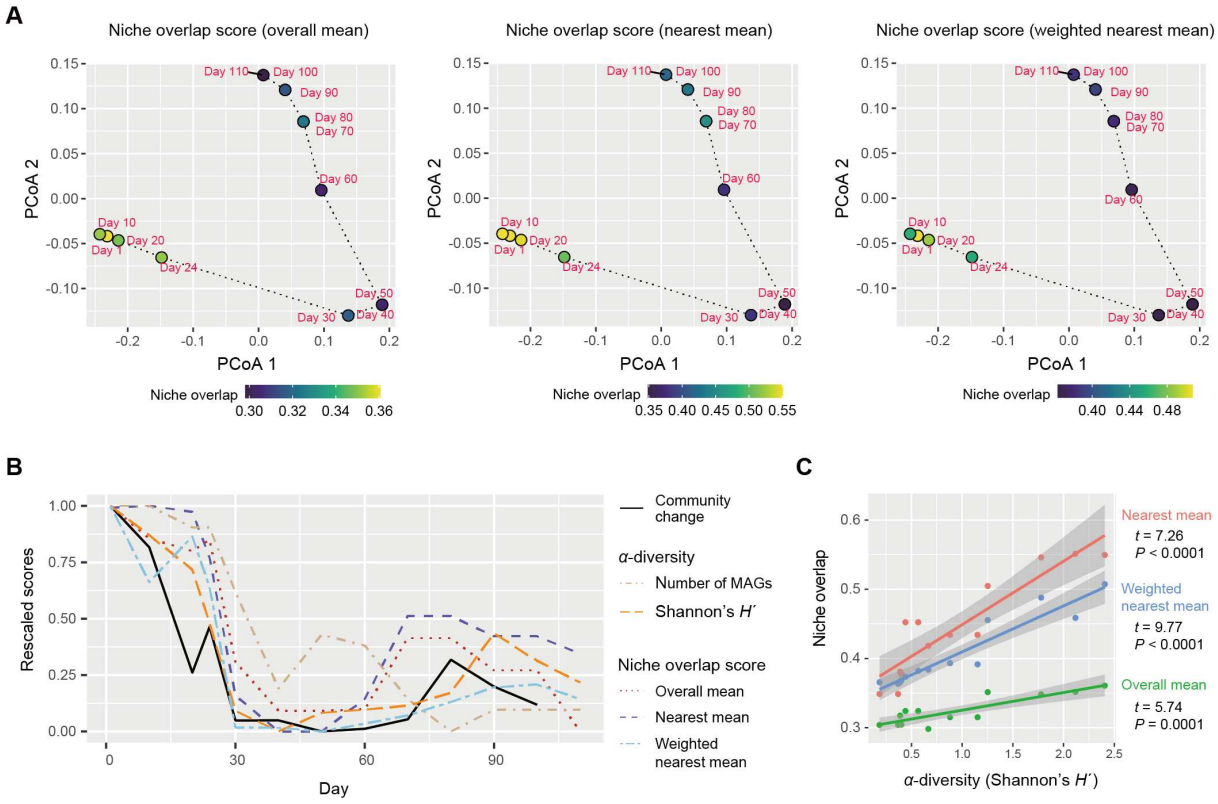

Fig. 4 Dynamics of niche-overlap level. **A** Community-level profiles of metabolic pathways/processes and niche overlap index. The niche overlap indices were defined based on the Jaccard similarity/dissimilarity of gene compositions between pairs of the microbial MAGs detected at a target time point. Three types of niche overlap indices are shown on a PCoA surface representing community-level compositions of genes. On the PCoA surface, time points are distributed based on the sum of the gene repertoires of the detected MAGs. **B** Dynamics of niche-overlap levels. Niche overlap scores are shown across the time-series. The magnitude of community compositional changes (Bray-Curtis β-diversity between present and next time points through the time-series of the shotgun metagenomic data) and α-diversity indices of the communities are shown as well. **C** Relationship between α-diversity and niche overlap scores. The lines represent linear regressions (with 95 % confidence intervals).

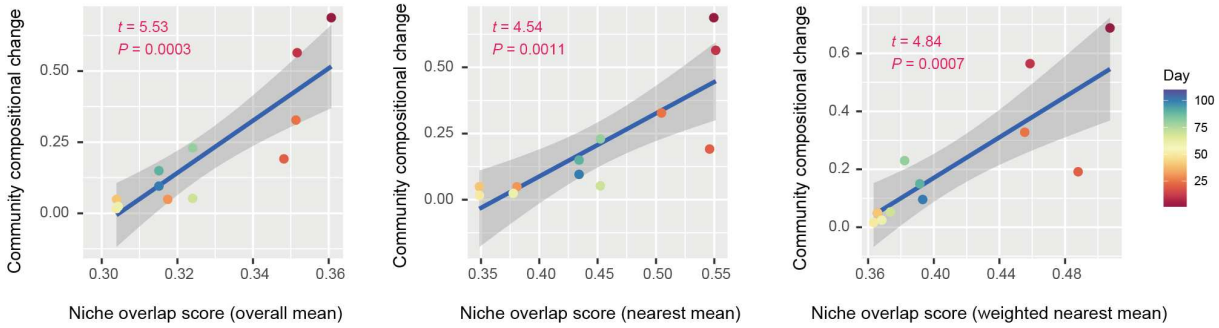

Fig. 5 Niche overlap level and community compositional shifts. The magnitude of community compositional changes observed in the microbiome was regressed on each niche overlap index obtained based on the shotgun metagenomic analysis. Niche overlap index at each time point and time-series shifts in community structure (Bray-Curtis β-diversity between present and next time points through the time-series of the shotgun metagenomic data) are shown along horizontal and vertical axes, respectively. The regression lines are shown with 95 % confidence intervals.